Fast Rotational Diffusion of Water Molecules in a 2D Hydrogen Bond Network at Cryogenic Temperatures

T. R. Prisk, C. Hoffmann, A. I. Kolesnikov, E. Mamontov, A. A. Podlesnyak, X. Wang, P. R. C. Kent, and L. M. Anovitz

Phys. Rev. Lett. **120**, 196001 — Published 9 May 2018

DOI: 10.1103/PhysRevLett.120.196001

Fast Rotational Diffusion of Water Molecules in a 2D Hydrogen Bond Network at Cryogenic Temperatures

T.R. Prisk*

Center for Neutron Research, National Institute of Standards and Technology, Gaithersburg, Maryland 208996-6100, USA

C. Hoffmann, A.I. Kolesnikov, E. Mamontov, A.A. Podlesnyak, and X. Wang

Neutron Scattering Division, Oak Ridge National Laboratory, Oak Ridge, Tennessee 37831, USA

P.R.C. Kent

Center for Nanophase Materials Sciences, Oak Ridge National Laboratory, Oak Ridge, Tennessee 37831, USA and Computational Sciences and Engineering Division, Oak Ridge National Laboratory, Oak Ridge, Tennessee 37831, USA

L.M. Anovitz

Chemical Sciences Division, Oak Ridge National Laboratory, Oak Ridge, Tennessee 37831, USA†

Abstract

Individual water molecules or small clusters of water molecules contained within microporous minerals present an extreme case of confinement where the local structure of hydrogen bond networks are dramatically altered from bulk water. In the zinc silicate hemimorphite, the water molecules form a two-dimensional hydrogen bond network with hydroxyl groups in the crystal framework. Here, we present a combined experimental and theoretical study of the structure and dynamics of water molecules within this network. The water molecules undergo a continuous phase transition in their orientational configuration analogous to a two-dimensional Ising model. The incoherent dynamic structure factor reveals two thermally activated relaxation processes, one on a subpicosecond time scale and another on a 10-100 ps time scale, between 70-130 K. The slow process is an in-plane reorientation of the water molecule involving breaking of hydrogen bonds with the framework that, despite the low temperatures involved, is analogous to rotational diffusion of water molecules in the bulk liquid. The fast process is a localized motion of the water molecule with no apparent analogs among known bulk or confined phases of water.

The physical and chemical properties of bulk liquid water are profoundly shaped by its hydrogen bond network[1]. Water molecules within the bulk liquid are, on average, tetrahedrally co-ordinated with their nearest neighbors. They undergo simultaneous translational and orientational (rotational) diffusion with characteristic relaxation times on the order of a few picoseconds. The structure and dynamics of liquid water are, however, strongly modified when it is adsorbed to a solid surface or confined within a porous material[2–5]. The translational dynamics of confined water are typically slowed by one or two orders of magnitude in comparison to the bulk liquid, with less severe consequences for the orientational diffusion. Water confined in porous silicas may be supercooled far below the bulk freezing temperature[6], resulting in increasingly glassy diffusive dynamics with characteristic relaxation times longer than a few hundred picoseconds at temperatures below 180-190 K. Two-dimensional, square ice forms on the surface of graphene and carbon nanotubes[7–9],while *para-ortho* transitions[10, 11] and tunneling states[12, 13] of ultra-confined water molecules have been observed.

Water molecules confined within microporous minerals present another extreme example of molecular confinement, where the local structure of H-bond networks formed by the water molecules may be strongly influenced by the surrounding framework. This opens the possibility of observing new types of dynamical and phase behavior. For example, hemimorphite $Zn_4Si_2O_7(OH)_2 \cdot H_2O$, a natural, orthorhombic, microporous zinc silicate, contains water molecules and hydroxyl groups that form a 2D H-bond network[14–19]. The crystal framework consists of rings of corner-sharing $ZnO_3(OH)$ and SiO_4 tetrahedra forming pore channels in the c-direction. The water molecule forms a two-dimensional network with the hydroxyl groups bound to the pore channels in the (010) plane. Previous diffraction studies[14, 20, 21] have found that, in Phase I ($T > 100$ K), the water molecule occupies a symmetrical position within the pore channels. It rests entirely upon the $a - c$ plane and forms four H-bonds with the framework. In Phase II ($T < 100$ K), there is an alternating system of rotated water molecules and hydroxyl groups forming a superlattice. There are only three, asymmetrically arranged H-bonds per water molecule.

In this Letter, we present a theoretical and experimental study of the phase behavior of hemimorphite and the dynamics of water molecules therein. We combined single-crystal neutron diffraction (ND) and quasi-elastic neutron scattering (QENS) measurements with density functional theory (DTF) calculations. The water molecules and framework hydroxyl

groups undergo an unusual order-disorder phase transition in their orientational configuration, highly reminiscent of a two-dimensional Ising model. They are highly mobile at cryogenic temperatures, in marked contrast to interfacial or confined water. Two types of local diffusive motion occur near 100 K: a planar analog to the rotation of water molecules in the bulk liquid, and a second with no known analog, suggesting a modification of the accepted crystal structure of hemimorphite.

Neutron diffraction and spectroscopy were performed at the Spallation Neutron Source at the Oak Ridge National Laboratory. Using the TOPAZ instrument[22] and CrystalPlan[23], we performed single crystal ND measurements at 90 K and 110 K that covered a full hemisphere in reciprocal space. QENS measurements on single crystal hemimorphite where carried out on the BASIS[24] and CNCS[25, 26] spectrometers using geometry described in Refs 27 and 28. Scattering data reduced and analyzed using VESTA[29], MantidPlot[30], and DAVE[31]. Technical details are provded in the Supporting Information.

Our ND measurements are in good agreement with previous studies of hemimorphite[14, 20, 21]. At 110 K, hemimorphite belongs to the space group $Imm2$ with $a = 8.3588$ Å, $b = 10.7283$ Å, and $c = 5.1065$ Å. H_2O forms a 2D H-bond network with the hydroxyl OH groups bound to the pore channels in the (010) plane.

We have fit the data collected at 110 K (Phase I) using two models for the H_2O position. According to Model A (Fig. 1(a)), there are four, symmetrically arranged coplanar H-bonds allowing the water molecule to act both as an acceptor and donor of H-bonds. At 90 K (Phase II, 1(b)), there are only three H-bonds per H_2O, and the oxygen atoms move slightly above or below the (010) plane. This is consistent with Raman spectroscopy measurements reporting low frequency bands (3300 cm^{-1} to 3500 cm^{-1}) along the c-axis while high frequency bands (3500 cm^{-1} to 3700 cm^{-1}) are present along the a-axis[18]. Model B for Phase I is the same as shown for Phase II with random occupancy of the water molecules. We regard the water molecule as donating only one H-bond because the bond angle deviates from colinearity by 9.3° for one hydrogen and by 40° for the other.

Model A provides an isotropic mean-squared displacement $\langle u^2_{iso} \rangle$ of approximately 0.08 $Å^2$, while Model B yields 0.02 $Å^2$.

At 90 K, hemimorphite belongs to the space group $Aem2$. As can be seen in Fig. 1(b), the framework undergoes little change as the mineral passes through the second-order phase transition at 100 K, aside from the size and shape of the displacement ellipsoids of the

framework atoms. There is an alternating system of rotated water molecules and hydroxyl groups forming a superlattice cell that doubles the b and c lattice parameters. The lattice parameters now are: $a = 8.3529$ Å, $b = 21.4590$ Å, and $c = 10.2147$ Å. As shown in Fig. 1(b), there are only three, asymmetrically arranged coplanar H-bonds acting on the water molecule.

To visualize the spatial disorder in this system, we calculated Fourier difference maps by including and excluding the water molecule and hydroxyl protons from the fully refined crystal structure. These maps generate nuclear density isosurfaces whose sizes and shapes represents the positions and displacements of the omitted atoms, in this case the water molecule and hydroxyl protons. These nuclear density isosurfaces are shown in Fig. 1 for both Phase I and Phase II.

Consistent sizes and shapes are obtained for the nuclear density isosurfaces at 110 K using Model A and Model B. Regardless of the choice of model, the nuclear density isosurfaces of the hydroxyl groups in Phase I are elongated ellipsoids that encompass their two possible positions in Phase II. The water oxygen and hydrogens have large displacements in all three spatial dimensions. When the crystal is cooled to Phase II, the elongated ellipsoids of the hydroxyl and water protons bifurcate into two distinct positions which they may occupy in the superlattice cell. As in Phase I, the nuclear density isosurfaces of Phase II reveal strong disorder of the water molecule and hydroxyl protons in every direction.

The displacement ellipsoids and nuclear density isosurfaces obtained in a diffraction experiment represent the time-averaged displacements of the atoms about their preferred positions. There is no information about whether these ellipsoids and isosurfaces are due to static or dynamic disorder (or both). Given the low temperatures involved, one is tempted to conclude that the disorder must only be static in nature. However, the mean-squared displacement of the water hydrogen, $\langle u^2 \rangle = 0.014$ Å^2, extracted from Q dependence of water intramolecular modes observed at SEQUOIA[26, 32] (to be described elsewhere; see also Supporting Information Figs 11 and 12), is inconsistent with the displacement parameters obtained from Model A and consistent with those of Model B.

The QENS data obtained at BASIS and CNCS also weigh against the static hypothesis. Figure 2 (a) plots a representative sample of the dynamic structure factor $S(\mathbf{Q}, E)$ at $T =$ 100 K obtained *via* BASIS in the energy range ± 100 μeV. We fit $S(\mathbf{Q}, E)$ to the sum of a Dirac δ-function, a single Lorentzian, and a linear background, all convoluted with

the instrumental resolution function. Figures 2 (b) and (c) plot the intrinsic width of the Lorentzian component, $\Gamma(Q)$, in the $\mathbf{Q} \parallel a$ and $\mathbf{Q} \parallel c$ sample orientations, respectively, as a function of the momentum transfer vector $\mathbf{Q}$ (see the caption to the Fig. 2). The Q-independent width implies localized or rotational diffusion.

Measurements of $S(\theta, E)$ over a wider energy range were conducted *via* CNCS at an incident neutron energy of 3 meV and 12 meV. The observed quasi-elastic broadening was independent of scattering angle θ up to the precision of our measurements. To improve statistics and simplify the data analysis, we have integrated $S(\theta, E)$ over scattering angles from 10° to 135° to obtain $S_p(E)$ and from −10° to −50° to obtain $S_n(E)$ (see also Supporting Information).

Figure 3 illustrates the inelastic scattering functions $S_p(E)$ and $S_n(E)$ at $T = 100$ K. We fit the scattering to the sum of a Dirac δ-function, two Lorentzian components, and a sloping linear background, again convoluted with the instrumental resolution function. A poor fit is obtained when only one Lorentzian component is used.

The QENS data collected at BASIS and CNCS show that the disorder of the water protons is at least partly dynamic. Moreover, there are two different relaxation processes occurring, which we will refer to as "slow" and "fast." The characteristic relaxation times for these two processes as a function of temperature are shown in Fig. 4(a).

In the BASIS data, only the slow process contributes to the scattering. These relaxation times $\tau(T)$ exhibit Arrhenius-type behavior $\tau(T) = \tau_0 \exp(E_a/k_B T)$, where the activation energy E_a is 6.6(4) kJ/mol.

In contrast, both the slow and fast processes are found in the CNCS data. Between 70 K and 120 K, the relaxation time τ for the fast component is less than one picosecond. This is shorter than the rotational relaxation time in bulk liquid water, which is on the order of a few picoseconds. The small, but slighly positive, slope of the blue curve in Fig. 4(a) shows that the fast relaxation process has a weak temperature dependence. Its activation energy is 0.4(2) kJ/mol.

The relaxation times of the slow process estimated from the CNCS data are approximately four times shorter than those estimated from the BASIS data set. However, the resulting change in the prefactor τ_0 is an artifact produced by the instrumental energy resolution and it is frequently observed in neutron scattering studies of confined fluids. E_a is not affected by this change. Thus the orange and red curves in Fig. 4(a) are parallel to one another, an

indication that they in fact represent the same physical process.

It is likely that the underlying mechanism of the slow process is associated with the breaking of H-bonds between the confined water hydrogens and the framework oxygen atoms, given the value of E_a. The breaking of H-bonds in bulk liquid water[33, 34] obeys an Arrhenius law with an activation energy of 10 kJ/mol. As argued by Geiger and Dachs[16, 17], the H-bond strength in hemimorphite is intermediate between steam, on the one hand, and liquid water and Ice Ih, on the other. Therefore, it is reasonable that the Arrhenius activation energy E_a associated with the breaking of H-bonds in hemimorphite is close to, yet somewhat less than, the corresponding activation energy E_a in bulk liquid water.

Neither the relaxation times, nor the the activation energies E_a, of the fast and slow diffusive processes are sensitive to the phase transition at T_c. This implies that the number of H-bonds per water molecule is unchanged as the mineral passes through T_c. If the number of bonds did change (as required by Model A), one would expect this to alter the orientational potential experienced by the water molecules, which would result in a kin in a plot of $\ln(\tau)$ versus $1000/T$. Since this is inconsistent with the observed behavior, we infer that Model B is more appropriate for the description of the Phase I crystal structure.

To gain further insight into the location and motion of the water molecules, we performed DFT calculations of a 160 atom hemimorphite supercell ($8x(Zn_4Si_2O_7(OH)_2 \cdot H_2O)$) containing 8 water molecules (see Supporting Information). Our calculations used the plane wave pseudopotential projector augmented wave method as implemented in the VASP code[35–39]. We used the PBE functional[40] and the DFT+D2 van der Waals method[41]. Our initial calculations found a C_{2v} symmetry structure with the water molecules primarily lying in the $a-c$ plane. However, breaking the symmetry of this structure by further perturbing the water molecules, we found the lower energy structure shown in Fig. 4(b), with each water molecule canted. Within PBE+D2 the supercell energy is 179 meV lower (22 meV/water molecule) than the higher symmetry structure (101 meV lower in PBE, or 13 meV/water molecule).

The new structure in Fig. 4(b) shows H-bonding between each water oxygen and the nearest hydroxyl. Limited relaxation of the $Zn_4Si_2O_7$ framework occurs, with a maximum 0.09 Å displacement of Zn and Si. We were unable to stabilize structures consisting of a single canted water molecule, with all others symmetric, most likely due to this lattice coupling.

The calculated orientational barrier, shown in Fig. 4(c), suggests a straightforward physical interpretation of the two relaxation processes. The slow process is a two-dimensional analog to the rotational diffusion of water molecules in the bulk liquid. That is, the water molecule moves *via* rotational jump diffusion between the two deep minima of the orientational potential, the activation energy being set by the strength of the H-bond which must be broken in order for the water molecule to move from one orientation/angular position in the channels to the other. The fast process, occurring on a subpicosecond time scale, has no known analogs. This process seems to be associated with the secondary, shallow minimum in the orientational potential. There may be a short lived state where the water molecule is momentarily symmetrically poised in the channel.

In this Letter, we presented a theoretical and experimental study of the phase behavior of hemimorphite and the dynamics of water molecules therein. The second-order phase transition of hemimorphite is analogous to a two-dimensional Ising model[42], where the orientational positions of the water molecules and framework hydroxyl groups (tilted to the left or right) correspond to the spin directions. In Phase II, these spins (positions) are anti-correlated in the a direction (with increasing the order parameter with decreasing temperature), and in Phase I the spins are uncorrelated (corresponding to zero order parameter). There are two types of local diffusive motion at temperatures on the order of 100 K: the first is a planar analog to the rotation of water molecules in the bulk liquid, whereas the second (fast) motion has no known analog in either the bulk or confined liquid. We believe that the anomalously fast rotational diffusion of the water molecule in hemimorphite at cryogenic temperatures is due to the planar configuration of the H-bonds, which usually have a tetrahedral arrangement in bulk or confined water phases. Therefore, confined water with similar 2D hydrogen-bonded structure may also exhibit similar dynamic and phase behavior.

This material is based upon work supported by the U.S. Department of Energy, Office of Science, Office of Basic Energy Sciences, Chemical Sciences, Geosciences, and Biosciences Division. This research at Oak Ridge National Laboratory's Spallation Neutron Source was also sponsored by the Scientific User Facilities Division, Office of Basic Energy Sciences, U.S. Department of Energy. Research by PK was conducted at the Center for Nanophase Materials Sciences, which is a DOE Office of Science User Facility. This research used resources of the National Energy Research Scientific Computing Center, a DOE Office of

Science User Facility supported by the Office of Science of the U.S. Department of Energy under Contract No. DE-AC02-05CH11231.

* timothy.prisk@nist.gov

[1] Y. Marechal, *The Hydrogen Bond and the Water Molecule* (Elsevier, 2007).

[2] V. Buch and J. Devlin, *Water in Confining Geometries* (Springer, 2003).

[3] F. Kremer, *Dynamics in Geometrical Confinement* (Springer, 2014).

[4] L. Liang, R. Romano, and H. Schober, *Neutron Applications in Earth, Energy, and Environmental Sciences* (Springer, 2008).

[5] L. Qiang, J. Song, F. Besenbacher, and M. Dong, Accounts of Chemical Research **48**, 119 (2015).

[6] S.-H. Chen, F. Mallamce, C.-Y. Mou, M. Broccio, C. Corsaro, A. Faraone, and L. Liu, Proc. Natl. Acad. Sci. USA **103**, 12974 (2006).

[7] G. Algara-Siller, O. Lehtinen, F. C. Wang, R. R. Nair, U. Kaiser, H. A. Wu, A. K. Geim, and I. V. Grigorieva, Nature **519**, 443 (2015).

[8] A. I. Kolesnikov, J.-M. Zanotti, C.-K. Loong, P. Thiyagarajan, A. P. Moravsky, R. O. Loutfy, and C. J. Burnham, Phys. Rev. Lett. **93**, 035503 (2004).

[9] G. Reiter, C. Burnham, D. Homouz, P. M. Platzman, J. Mayers, T. Abdul-Redah, A. P. Moravsky, J. C. Li, C.-K. Loong, and A. I. Kolesnikov, Phys. Rev. Lett. **97**, 247801 (2006).

[10] C. Beduza, M. Carravettab, J.-C. Chenc, M. Concistreb, M. Denningb, M. Frunzic, A. Horsewilld, O. Johannessenb, R. Lawlere, X. Leic, M. Levittb, L. Lic, S. Mamoneb, Y. Murataf, U. Nagelg, T. Nishidaf, J. Ollivierh, S. Rolsh, T. Room, R. Sarkarb, N. Turroc, and

Y. Yanga, P. Natl. Acad. Sci. USA **109**, 12894 (2012).

[11] K. S. K. Goh, M. Jiménez-Ruiz, M. R. Johnson, S. Rols, J. Ollivier, M. S. Denning, S. Mamone, M. H. Levitt, X. Lei, Y. Li, N. J. Turro, Y. Murata, and A. J. Horsewill, Phys. Chem. Chem. Phys. **16**, 21330 (2014).

[12] A. I. Kolesnikov, G. F. Reiter, N. Choudhury, T. R. Prisk, E. Mamontov, A. Podlesnyak, G. Ehlers, A. G. Seel, D. J. Wesolowski, and L. M. Anovitz, Phys. Rev. Lett. **116**, 167802 (2016).

[13] B. P. Gorshunov, E. S. Zhukova, V. I. Torgashev, V. V. Lebedev, G. S. Shakurov, R. K. Kremer, E. V. Pestrjakov, V. G. Thomas, D. A. Fursekno, and M. Dressel, J. Phys. Chem. Lett. **4**, 2015 (2013).

[14] E. Libowitzky, A. J. Schultz, and D. M. Young, Z. Kristallogr. **213**, 659 (1998).

[15] E. Libowitzky and G. R. Rossman, Am. Mineral. **82**, 1111 (1997).

[16] C. A. Geiger and E. Dachs, Am. Mineral. **94**, 634 (1994).

[17] E. Dachs and C. A. Geiger, Eur. J. Mineral. **5**, 971 (2009).

[18] B. Kolesov, Am. Mineral. **91**, 1355 (2006).

[19] M. Mao, Z. Li, and Y. Pan, Phys. Chem. Minerals **40**, 133 (2013).

[20] R. J. Hill, G. V. Gibbs, J. R. Craig, F. K. Ross, and J. M. Williams, Z. Kristallogr. **146**, 241 (1977).

[21] Y. Takéuchi, S. Sasaki, W. Joswig, and H. Fuess, Proc. Japan Acad. Sci. **54**, 577 (1978).

[22] M. R. V. Jørgensen, V. R. Hathwar, M. Sist, X. Wang, C. M. Hoffmann, A. L. Briseno, J. Overgaard, and B. B. Iversen, Acta Cryst. A **70**, 679 (2014).

[23] J. Zikovsky, P. F. Peterson, X. P. Wang, M. Frost, and C. Hoffmann, J. Appl. Crystal. **44**, 418 (2011).

[24] E. Mamontov and K. W. Herwig, Rev. Sci. Instrum. **82**, 85109 (2011).

[25] G. Ehlers, A. A. Podlesnyak, J. L. Niedziela, E. B. Iverson, and P. E. Sokol, Rev. Sci. Instrum. **82**, 085108 (2011).

[26] M. B. Stone, J. L. Niedziela, D. L. Abernathy, L. DeBeer-Schmitt, G. Ehlers, I. Garlea, G. E. Granroth, M. Graves-Brook, A. I. Kolesnikov, A. A. Podlesnyak, and B. Winn, Rev. Sci. Instrum. **85**, 045113 (2014).

[27] L. M. Anovitz, E. Mamontov, P. ben Ishai, and A. I. Kolesnikov, Phys. Rev. E **88**, 052306 (2013).

[28] A. I. Kolesnikov, L. M. Anovitz, E. Mamontov, A. A. Podlesnyak, and G. Ehlers, J. Phys. Chem. B **118**, 13414 (2014).

[29] K. Momma and F. Izumi, J. Appl. Crystallogr. **44**, 1272 (2011).

[30] O. Arnold, J. Bilheux, J. Borreguero, A. Buts, S. Campbell, L. Chapon, M. Doucet, N. Draper, R. F. Leal, M. Gigg, V. Lynch, A. Markvardsen, D. Mikkelson, R. Mikkelson, R. Miller, K. Palmen, P. Parker, G. Passos, T. Perring, P. Peterson, S. Ren, M. Reuter, A. Savici, J. Taylor, R. Taylor, R. Tolchenov, W. Zhou, and J. Zikovsky, Nuclear Instruments and Methods in Physics Research Section A: Accelerators, Spectrometers, Detectors and Associated Equipment **764**, 156 (2014).

[31] R. T. Azuah, L. R. Kneller, Y. Qiu, P. L. W. Tregenna-Piggott, C. M. Brown, J. R. D. Copley, and R. M. Dimeo, J. Res. Natl. Inst. Stan. Technol. **114**, 341 (2009).

[32] G. E. Granroth, A. I. Kolesnikov, T. E. Sherline, J. P. Clancy, K. A. Ross, J. P. C. Ruff, B. D. Gaulin, and S. E. Nagler, J. Phys. Conf. Ser. **251**, 012058 (2010).

[33] O. Conde and J. Teixeira, J. Phys. (Paris) **44**, 525 (1983).

[34] C. J. Montrose, J. A. Bucaro, J. Marshall, and T. A. Litovitz, J. Chem. Phys. **60**, 5025 (1974).

[35] G. Kresse and J. Hafner, Physical Review B **47**, 558 (1993).

[36] G. Kresse and J. Hafner, Physical Review B **49**, 14251 (1994).

[37] G. Kresse and J. Furthmuller, Computational Materials Science **6**, 15 (1996).

[38] G. Kresse and J. Furthmuller, Physical Review B **54**, 11169 (1996).

[39] G. Kresse and D. Joubert, Physical Review B **59**, 1758 (1999).

[40] J. P. Perdew, K. Burke, and M. Ernzerhof, Physical Review Letters **77**, 3865 (1996).

[41] S. Grimme, J. Antony, S. Ehrlich, and H. Krieg, Journal of Chemical Physics **132**, 154104 (2010).

[42] P. Anderson, *Basic Notions of Condensed Matter Physics*, Advanced Book Classics (Westview Press, 1997).

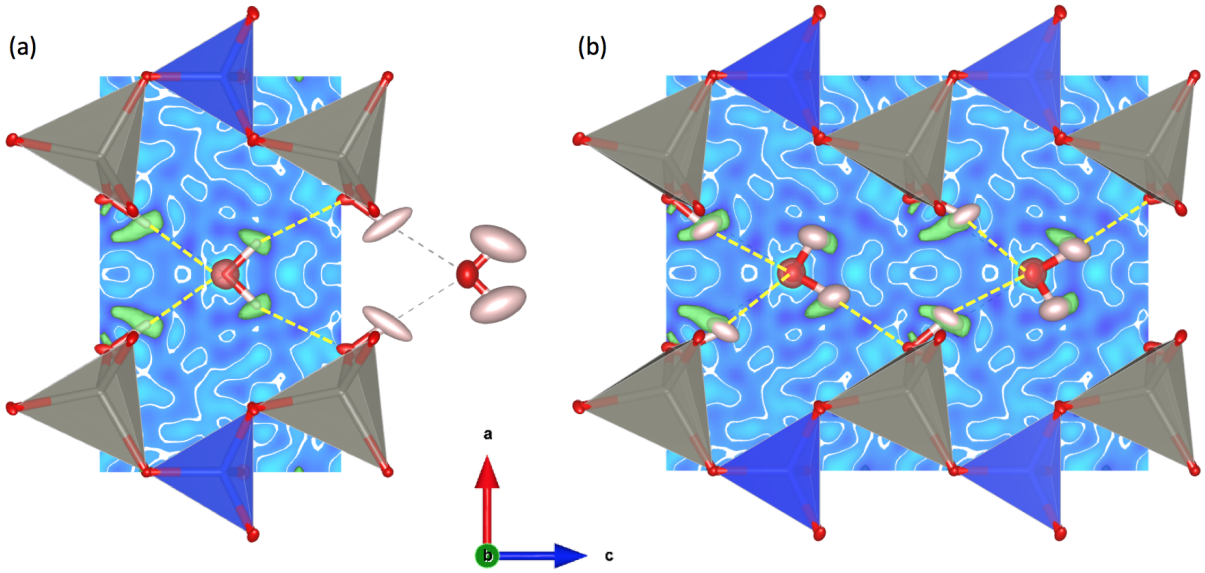

FIG. 1. The crystal structure of hemimorphite viewed along the b-axis. The framework is shown as a traditional ball-and-stick model with anisotropic displacement parameters at 65% probability. The hydroxyl proton and the water molecule are shown as nuclear density isosurfaces. Panel (a) illustrates Model A for Phase I and panel (b) illustrates the unit cell for Phase II. Model B for Phase I is the same as shown on panel (b) with random occupancy of the water molecules. Figure designations: nuclear density isosurfaces for water oxygens (red); nuclear density isosurfaces for water or hydroxyl protons (green); SiO_4 tetrahedra (blue); $ZnO_3(OH)$ tetrahedra (gray); framework oxygen (red).

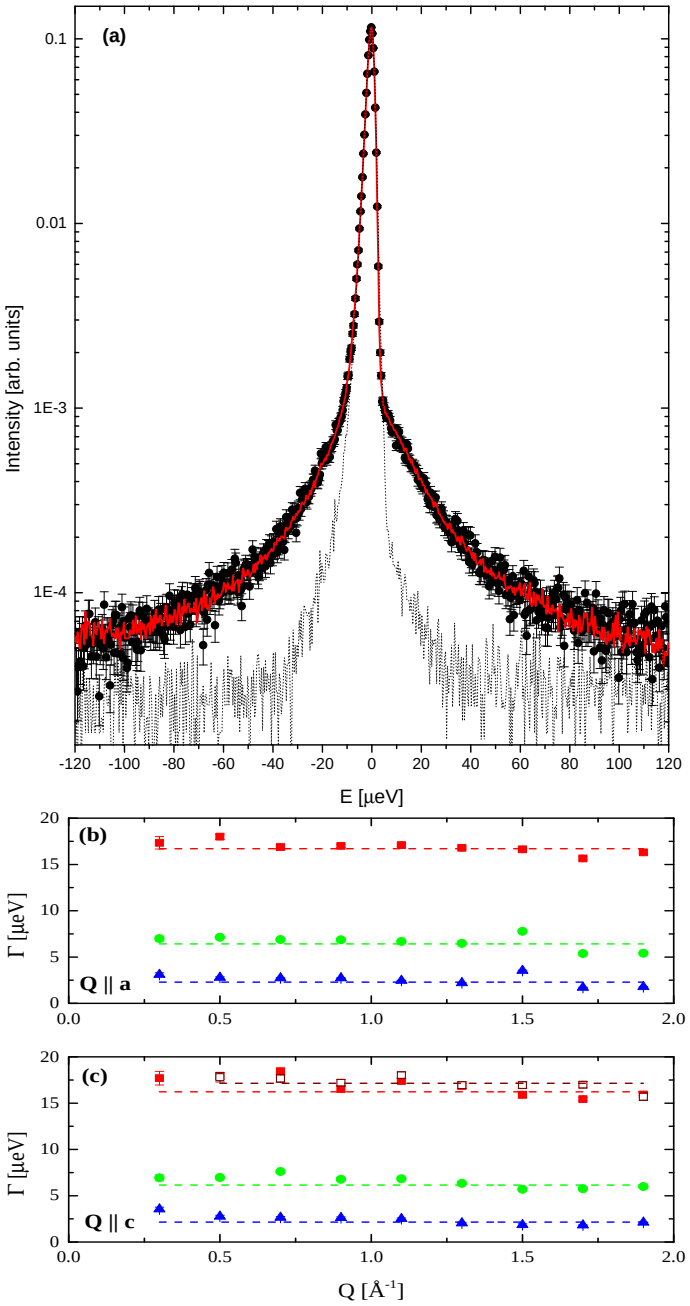

FIG. 2. Panel (a) illustrates BASIS measurements of the dynamic structure factor $S(Q, E)$ of hemimorphite at $T = 100$ K when $\mathbf{Q} \parallel c$ and $Q = 1.50$ Å^{-1}. The intrinsic half-width at half-maximum Γ of the Lorentzian component observed at BASIS is shown in panels (b) and (c). Solid symbols in both panels show the observed widths when $Q = 0.70$ Å^{-1} is exactly parallel to the the specified crystal direction. The blue, green, and red symbols correspond to 80 K, 90 K, and 100 K, respectively. Open symbols in (c) plot the intrinsic widths Γ when $Q = 1.50$ Å^{-1} is exactly parallel to c. Error bars throughout the text represent one standard deviation.

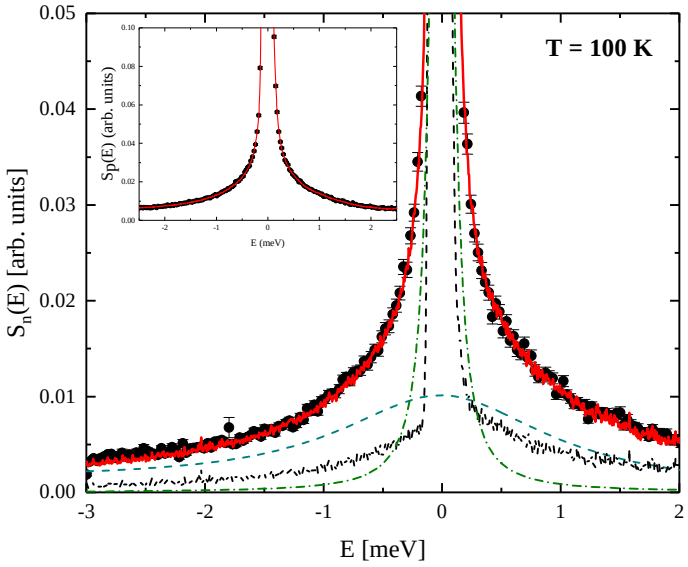

FIG. 3. The observed inelastic scattering function $S(E)$ obtained *via* CNCS. A fit to the scattering data from the negative-angle detectors with the following symbol designations: experimental data (black circles); broad Lorentzian component plus linear background (dashed dark cyan line); narrow Lorentzian component (dashed-dotted green line); elastic scattering (dotten black line); and total fit function (solid red curve). The insert plots the data from the positive-angle detectors.

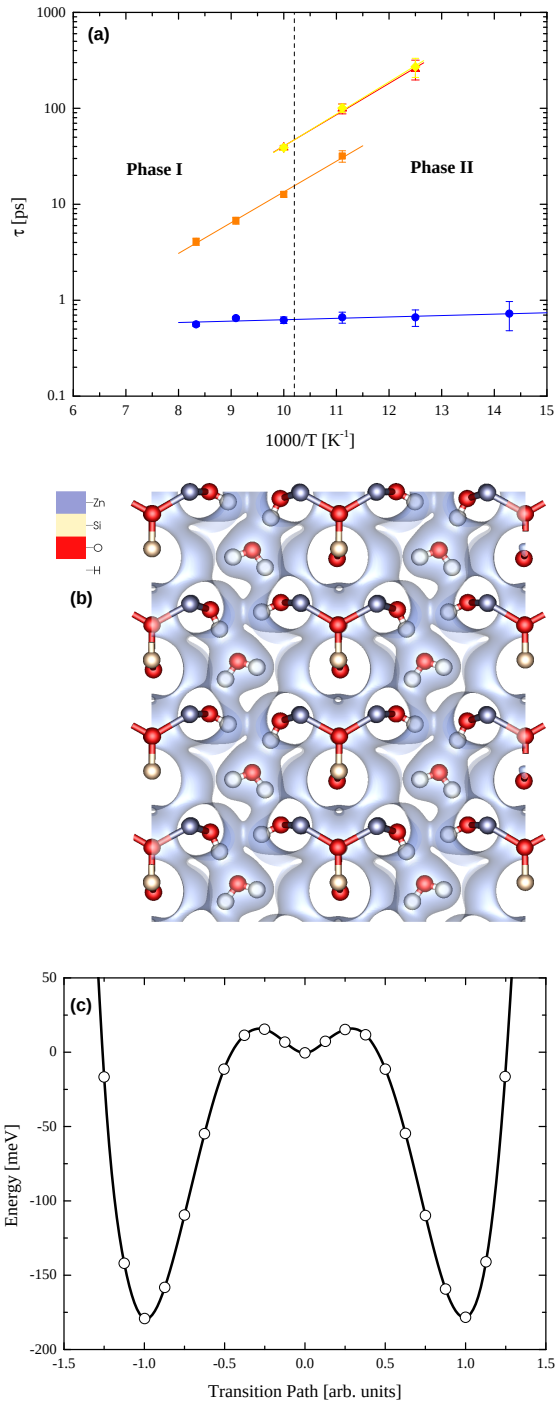

FIG. 4. Panel (a) is an Arrhenius plot of the proton relaxation times τ. These were obtained from: the BASIS spectrometer, for the slow components on the *ab*-plane (red triangles) and on the *ac*-plane (yellow diamonds), and from the CNCS spectrometer, for the slow component on the *bc*-plane (orange squares), and the fast component on the *bc*-plane (blue circles). Panel (b) shows the cross-section of the DFT structure and isosurface of the electronic charge density illustrating the in-plane alternating layout of the water molecules. Panel (c) plots the orientational potential barrier of eight water molecules obtained from the DFT calculations.